A Sensitive Differential Capacitance to Voltage Converter for Sensor Applications

Joost C. Lötters, Wouter Olthuis, Peter H. Veltink, *Member, IEEE,* and Piet Bergveld

***Abstract*—There is a need for capacitance to voltage converters (CVC's) for differential capacitive sensors like pressure sensors and accelerometers which can measure both statically and dynamically. A suitable CVC is described in this paper. The CVC proposed is based on a symmetrical structure containing two half ac bridges, is intrinsically immune to parasitic capacitances and resistances, is capable of detecting capacitance changes from dc up to at least 10 kHz, is able to handle both single and differential capacitances, and can easily be realized with discrete components. Its sensitivity is very high: detectable capacitance changes of the order of 2 ppm of the nominal value (24 aF with respect to a nominal capacitance of 12 pF) result in a measured output voltage of 1.5 mV. However, due to drift the absolute accuracy and resolution of the CVC is limited to 3.5 ppm. A differential accelerometer for biomedical purposes was connected to the CVC and showed a sensitivity of 4 V/g. The measured rms output voltage noise in the frequency range of 2–50 Hz is 750 μV, resulting in a signal to noise ratio of 75 dB at an acceleration of 1 g in the frequency range of 2–50 Hz.**

***Index Terms*— Capacitive accelerometer, (differential) capacitance to voltage converter, differential measurement, Pspice simulations.**

I. Introduction

SINCE capacitive sensors are becoming more and more popular, many methods [1]–[6] have been introduced which deal with the conversion of capacitance values into a voltage. Most methods are not capable of handling very small variations of the order of 1 ppm of the nominal capacitance value [3], [4]. Some of them, for instance the method which uses an integrator [3], are not capable of handling static capacitances. Others, for instance the modified Martin oscillator with microcontroller or the switched-capacitor interface [4], [5], are not capable of handling capacitance changes with frequencies higher than 10 Hz. Another method is based on the ratio-arm bridge circuit [6] which is symmetrical and very sensitive, but this method has the disadvantage that transformer coils have to be used which may be a problem when the circuit has to be integrated.

This paper presents a differential capacitance to voltage converter (CVC) which does not show the limitations as mentioned above and is easy to realize with discrete components. Furthermore, the CVC consists of a symmetrical circuit, so undesired common mode interference is rejected. The CVC is designed to match a differential capacitive acceleration sensor for biomedical purposes [7] but can be used in many other sensor types like differential capacitive pressure sensors.

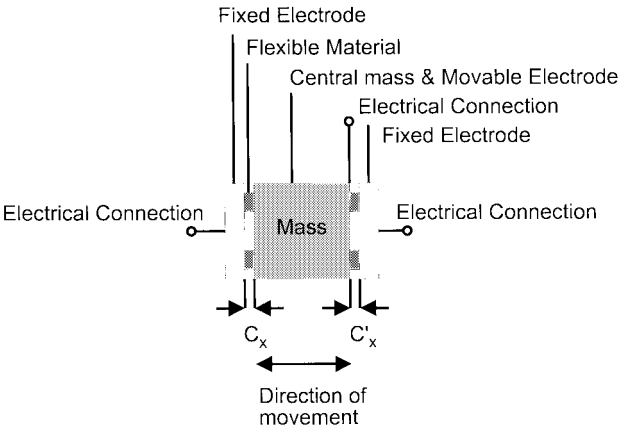

Fig. 1. Basic structure of the differential capacitive acceleration sensor.

The basic structure of the differential capacitive acceleration sensor [8], [9] is shown in Fig. 1. The two sensor capacitances C_x and C'_x, which have nominal values $C_x = C_{x0}$ and $C'_x = C'_{x0}$, respectively, are equal when there is no lateral acceleration: $C_{x0} = C'_{x0}$. When an acceleration is applied, the central mass moves with respect to the fixed electrodes and the two capacitances change. For instance, when the mass moves to the left with respect to the fixed electrodes, the left capacitance increases with ΔC_x and the right capacitance decreases with $\Delta C'_x$, so the differential capacitance change is $C_x - C'_x = C_{x0} + \Delta C_x - (C'_{x0} - \Delta C'_x) = 2\Delta C_x$, when $\Delta C_x = \Delta C'_x$.

The accelerometer is used for biomedical purposes such as detection of movements of the extremities. With the present design, the nominal capacitance value C_{x0} is about 12 pF. The accelerometer has the following specifications:

- the frequency range of the change in acceleration is dc to 50 Hz;
- the minimum detectable change in acceleration is ±0.001 g, corresponding to a capacitance change $\Delta C_{x,\min} = \pm 24$ aF (±2 ppm of 12 pF);
- the maximum change in acceleration is ±5 g, corresponding to a capacitance change $\Delta C_{x,\max} = \pm 120$ fF (±1% of 12 pF).

Manuscript received July 18, 1996; revised January 11, 1999. This work was supported by the Dutch Technology Foundation (STW).

J. C. Lötters is with Bronkhorst High-Tech, 7261 AK Ruurlo, The Netherlands.

W. Olthuis and P. Bergveld are with the MESA Research Institute, 7500 AE Enschede, The Netherlands (e-mail: w.olthuis@el.utwente.nl).

P. H. Veltink is with BMTI, University of Twente, 7500 AE Enschede, The Netherlands.

Publisher Item Identifier S 0018-9456(99)02850-8.

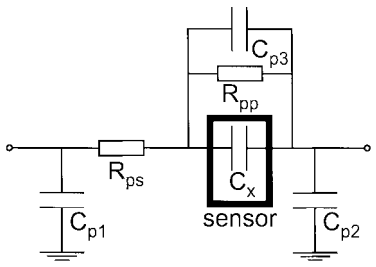

Fig. 2. Sensor capacitance C_x with the parasitic capacitances C_{p1} and C_{p2} at its terminals, C_{p3} in parallel with the sensor and the parasitic resistances R_{pp} in parallel and R_{ps} in series with the sensor.

Since the rms change in capacitance due to mechanical thermal noise of the sensor in the signal bandwidth of dc 50 Hz is negligible with respect to $\Delta C_{x,\min}$, the noise behavior of the CVC should be modeled and minimized such that the resulting output noise voltage does not exceed the output voltage due to $\Delta C_{x,\min}$.

The measurement of a sensor capacitance often has to deal with parasitic capacitances of the same order of magnitude as the nominal sensor capacitance and is, in addition, also very sensitive to electromagnetic interference. Furthermore, due to the sensor structure undesired parasitic resistances may appear in parallel or in series with the sensor capacitance. Both the sensor capacitance C_x [F] and the parasitic capacitances C_{p1}, C_{p2}, and C_{p3} and resistances R_{pp} [Ω] and R_{ps} are shown in Fig. 2.

Impedance measurements (HP 4194A impedance/gain phase analyzer) on the realized sensor as shown in Fig. 1 showed that the parasitic capacitances are all approximately 3 pF, the parasitic parallel resistance $R_{pp} > 200$ MΩ and the series resistance $R_{ps} \approx 0.5\,\Omega$. The CVC should be immune to the parasitic components to obtain an output voltage which is only dependent on the sensor capacitance C_x.

In this paper, a CVC design is proposed and a theoretical description of the transfer function and the noise behavior is given. The results of both computer simulations (PSPICE) and measurements are described and discussed. Finally, the conclusions are drawn and some recommendations for possible improvements are given.

II. Theory

A. Circuit Description

The basic circuit of the differential capacitance to voltage converter is shown in Fig. 3. The CVC is completely symmetrical and consists of two frequency independent half ac-bridges which act as AM modulators, two AM demodulators, and an instrumentation amplifier which rejects common mode signals.

In Fig. 3, one of the electrodes of the variable sensor capacitance C_x is connected to a voltage source providing an excitation voltage $V_{carrier}$ with a carrier frequency $f_{carrier}$ [Hz] and amplitude $V^{carrier}$ [V], and the other one to the input of a current detector (which is at virtual ground potential) with a very low input impedance. The parasitic capacitances C_{p1} and C_{p2}, as shown in Fig. 2, are in parallel with the voltage source and the low input impedance of the current detector, respectively, thus having virtually no effect on the measurement of the current flowing through C_x. The effect of the parasitic capacitance C_{p3} parallel to the sensor capacitance can be eliminated by offset nulling and/or differential measurement, provided that its value remains constant and/or is equal in both halves of the circuit.

The parasitic resistors R_{pp} and R_{ps} introduce both a high and a low cutoff frequency in the transfer function of $V_{carrier}$ to V_A, as will be shown in (1)–(6). For frequencies between both cutoff frequencies, the transfer function is independent of the parasitic resistors. So, when the operating carrier frequency $f_{carrier}$ is chosen such that it is between the cutoff frequencies imposed by the parasitic resistors, the parasitic resistors will not affect the behavior of the circuit.

The same reasoning is valid for the transfer of $V_{carrier}$ to V_B. In the remainder of this paper, only one half of the circuit will be described, since the other half is expected to behave the same way.

The feedback resistor R_f provides the negative input of the opamp with the necessary dc bias current. Together with the feedback capacitor C_f this resistor acts as a high-pass filter with a certain cutoff frequency. In order to be sure that the carrier voltage is unaffected by the high-pass filter, R_f should be as high as possible so that the resulting cutoff frequency is much lower than $f_{carrier}$.

When no acceleration is applied, C_f is chosen such that it equals C_{x0} and consequently the transfer function from $V_{carrier}$ to V_A will be -1. When a certain acceleration occurs, the value of C_x changes and the transfer function will show small variations around -1 due to the very small value of $\Delta C_x/C_{x0}$. Thus, the input voltage is amplitude modulated (AM) by the variation in the sensor capacitance.

The transfer function of $V_{carrier}$ to V_A, considering the sensor representation of Fig. 2 and the CVC of Fig. 3

$$\frac{V_A}{V_{carrier}} = -\frac{R_f}{R_{pp}+R_{ps}} \cdot \frac{1+j\omega R_{pp}(C_x+C_{p3})}{(1+j\omega R_f C_f)\left(1+j\omega\,\dfrac{R_{pp}R_{ps}}{R_{pp}+R_{ps}}\,(C_x+C_{p3})\right)}. \tag{1}$$

This transfer function is frequency independent when the input voltage $V_{carrier}$ has a frequency $f_{carrier}$ which satisfies the following conditions

$$f_{carrier} \gg \frac{1}{2\pi R_f C_f} \tag{2}$$

$$f_{carrier} \gg \frac{1}{2\pi R_{pp}(C_x+C_{p3})} \tag{3}$$

$$f_{carrier} \ll \frac{R_{pp}+R_{ps}}{2\pi R_{pp}R_{ps}(C_x+C_{p3})}. \tag{4}$$

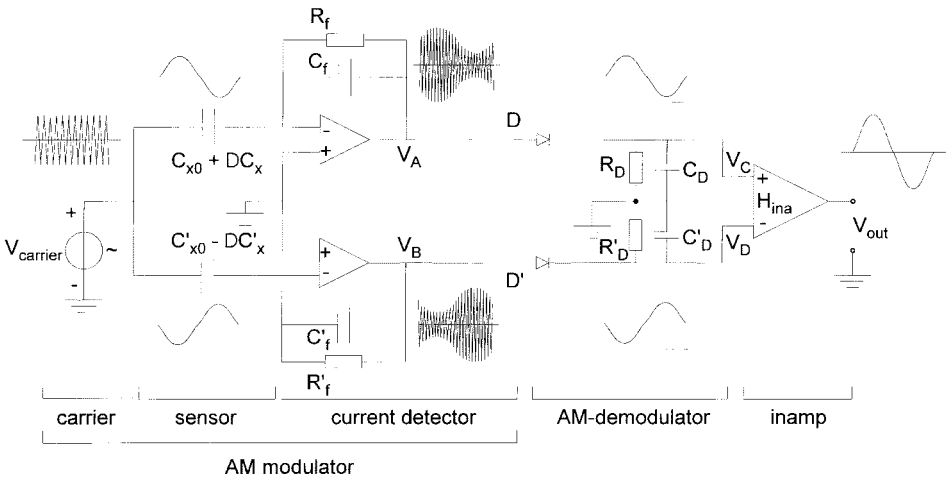

Fig. 3. Basic circuit of the differential capacitance to voltage converter including typical signal waveforms.

Thus, by choosing $f_{carrier}$ according to (2)–(4), at that certain range of $f_{carrier}$ (1) can be rewritten as

$$\frac{V_A}{V_{carrier}} = -\frac{R_{pp}}{R_{pp}+R_{ps}} \cdot \frac{C_x + C_{p3}}{C_f} \approx -\frac{C_x + C_{p3}}{C_f}. \quad (5)$$

It can be seen that V_A is an AM signal, since $f_{carrier}$ of $V_{carrier}$ is a high frequency carrier and C_x varies due to accelerations with low frequency f_{signal} such that $C_x = C_{x0}(1 + (\Delta C_x/C_{x0}) \cos \omega_{signal} t)$. Substitution of this last equation in (5) yields

$$V_A \approx -\frac{C_{x0}\left(1 + \frac{\Delta C_x}{C_{x0}} \cdot \cos \omega_{signal} t\right)}{C_f} \hat{V}_{carrier} \cdot \cos \omega_{carrier} t - \frac{C_{p3}}{C_f} \hat{V}_{carrier} \cos \omega_{carrier} t. \quad (6)$$

The AM signal is demodulated in the rectifier circuit, consisting of a diode D with diode voltage drop V_{diode} and an RC-circuit with resistor R_D and capacitor C_D. The $R_D C_D$ time constant of the demodulator should be chosen so that the input frequency $f_{carrier}$ is eliminated and the sensor signal with frequency f_{signal} is transferred unaffectedly

$$f_{signal} \ll \frac{1}{2\pi R_D C_D} \ll f_{carrier}. \quad (7)$$

A general equation will be derived with which the maximum bandwidth of the demodulator circuit can be calculated. The minimum cutoff frequency $f_{-3\,\mathrm{dB,\,min}}$ [Hz] of the demodulator is given by

$$f_{-3\,\mathrm{dB,\,min}} = \frac{1}{2\pi R_D C_D}. \quad (8)$$

The ripple voltage V_{ripple} [V]

$$\hat{V}_{ripple} \approx \frac{\hat{V}_{carrier}}{R_D C_D f_{carrier}} \quad (9)$$

with slope S_{ripple} [V/s]

$$S_{ripple} = \frac{\hat{V}_{carrier}}{R_D C_D}. \quad (10)$$

due the decharging of C_D over R_D when the diode is reverse biased, is a measure for the maximum signal frequency, because the maximum negative slope of the signal will be limited by the slope of the ripple: when the negative signal slope is steeper than the ripple slope, the diode will remain reverse biased and the signal will not be transferred. The negative signal slope S_{signal} [V/s] is given by

$$S_{signal} = \hat{V}_{signal} \omega_{signal}. \quad (11)$$

By equating the ripple slope and the signal slope and assuming that the diode is forward biased (which is the case when $V_{diode} >= 300$ mV), the following expression can be derived for maximum cutoff frequency $f_{-3\,\mathrm{dB,\,max}}$ [Hz]

$$f_{-3\,\mathrm{dB,\,max}} = K \cdot \frac{\hat{V}_{carrier}}{2\pi R_D C_D \hat{V}_{signal}} \quad (12)$$

where K is a dimensionless gain factor which depends on the components used and the structure of the circuit.

After demodulation, the resulting voltages V_C and V_D are

$$V_C = \hat{V}_A - V_{diode} \quad (13)$$

$$V_D = \hat{V}_B - V'_{diode}. \quad (14)$$

Subsequently, the difference between V_C and V_D is amplified by the instrumentation amplifier (inamp) with gain factor H_{ina}. The inamp eliminates common-mode voltages, such as that introduced by two equal parasitic capacitances C_{p3} and V_{diode}. The output voltage V_{out} of the CVC can be calculated with

$$V_{\mathrm{out}} = H_{ina} \cdot (V_C - V_D) \quad (15)$$

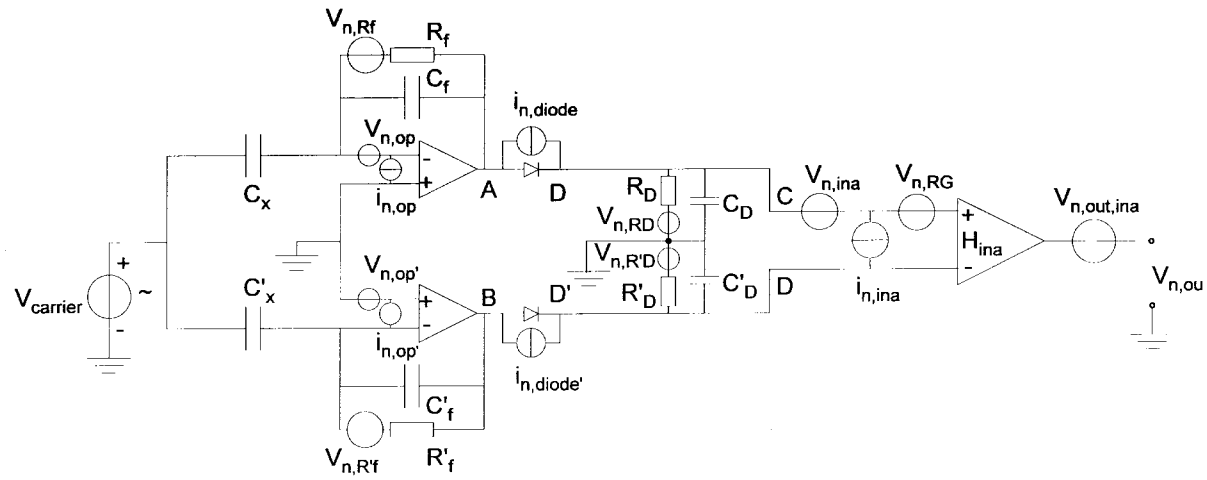

Fig. 4. Capacitance to voltage converter with its noise sources.

$$V_{\text{out}} = -H_{ina}\left[\hat{V}_{carrier}\left(\frac{R_{pp}}{R_{pp}+R_{ps}} \cdot \frac{C_{p3}+C_{x0}+\Delta C_x \cos\omega_{signal}t}{C_f} - \frac{R'_{pp}}{R'_{pp}+R'_{ps}} \cdot \frac{C'_{p3}+C'_{x0}-\Delta C'_x \cos\omega_{signal}t}{C'_f}\right) - V_{diode}+V'_{diode}\right]. \tag{16}$$

This expression can be simplified into

$$V_{\text{out}} = -H_{ina}\hat{V}_{carrier}\frac{2\Delta C_x \cos\omega_{signal}t}{C_f} \tag{17}$$

when $R_{pp} \gg R_{ps}, R'_{pp} \gg R'_{ps}$, $C_{p3} = C'_{p3}$, $C_{x0} = C'_{x0}$, $\Delta C_x = \Delta C'_x$, and $V_{diode} = V'_{diode}$. When $C_{p3} \neq C'_{p3}$, $C_{x0} \neq C'_{x0}$, $\Delta C_x \neq \Delta C'_x$, and $V_{diode} \neq V'_{diode}$, the inequalities will cause an offset shift in the expression which can be eliminated by offset nulling. The gain-bandwidth product of the inamp should be sufficiently high to guarantee that the maximum bandwidth of the demodulation circuit can be obtained.

The significance of (17) for the accelerometer case is that $V_{\text{out}} = 0$ when the device experiences no acceleration ($\Delta C_x = 0$) and $V_{\text{out}} \neq 0$ when an acceleration is applied.

B. Noise Behavior of the Capacitance to Voltage Converter

The capacitance to voltage converter with its noise sources is shown in Fig. 4.

The output noise voltage of the current detector at A is called $V_{n,A}$ and at B $V_{n,B}$. It can be shown that the spectral density of the noise voltage at A is equal to

$$\frac{V^2_{n,A}}{\Delta f} = \frac{V^2_{n,opamp}}{\Delta f} \cdot \frac{1+\omega^2_{carrier}R^2_f(C_x+C_f+C_{p2}+C_{p3})^2}{1+\omega^2_{carrier}R^2_fC^2_f} + \frac{i^2_{n,opamp}}{\Delta f} \cdot \frac{R^2_f}{1+\omega^2_{carrier}R^2_fC^2_f} + \frac{V^2_{n,Rf}}{\Delta f} \cdot \frac{1}{1+\omega^2_{carrier}R^2_fC^2_f}. \tag{18}$$

From this equation it can be seen that in order to obtain a low output noise voltage, a fairly high operating frequency $f_{carrier}$ should be used and the parasitic capacitances should be as small as possible. The feedback resistor, R_f, should be large to decrease its own noise voltage in combination with C_f, but should be small to decrease the effect of the current noise of the opamp, so an optimum should be found. A similar equation can be derived for $V_{n,B}$.

Since all noise sources are assumed to be uncorrelated and the CVC is symmetrical it can be concluded that $V^2_{n,A} = V^2_{n,B}$.

The demodulator circuit consists of a diode D, a resistor R_D, and a capacitor C_D. The resistor produces a thermal noise voltage $V_{n,RD} = \sqrt{(4kTR_D\Delta f)}$. The diode is considered to behave as a shot noise source which can be modeled as a noise current source $i_{n,diode}$ [A]. The equivalent noise current of the diode can be calculated with [10]

$$\frac{i^2_{n,diode}}{\Delta f} = 2qI_D \tag{19}$$

where q is the electron charge, $q = 1.6 \times 10^{-19}$ [C], and I_D is the dc current through the diode.

Both diodes in the CVC are assumed to have the same noise power, $i^2_{n,diode} \approx i^{2'}_{n,diode}$. However, the diode noise current can be neglected with respect to the other noise sources in the circuit.

The noise of the inamp can be represented by an equivalent input noise voltage source $V_{n,ina}$ and an equivalent noise current source $i_{n,ina}$ at the input terminals of the inamp. Other noise sources, such as the—uncorrelated—equivalent output noise voltage $V_{n,ina,\text{out}}$ and the thermal noise voltage $V_{n,RG} = \sqrt{(4kTR_G\Delta f)}$ of the resistor R_G which determines the gain are only important for inamps with extremely low input noise voltage levels.

For the calculation of the total output noise voltage, the two possible diode states have to be examined. When the diode is reverse biased, both the signal and the noise of the input opamps are not transferred by the demodulator circuit due to the high resistance r_{diode} [Ω] of the diode: $r_{diode} \approx \infty$. In this

case, the output noise voltage is given by

$$\frac{V_{n,\mathrm{out},rb}^2}{\Delta f} = \frac{V_{n,\mathrm{out},ina}^2}{\Delta f} + H_{ina}^2 \cdot \left[\frac{4kTR_G}{\Delta f} + 2\left(\frac{V_{RD}^2}{\Delta f} \cdot \frac{1}{1+\omega^2 R_D^2 C_D^2} + \left(\frac{i_{n,diode}^2}{\Delta f} + \frac{i_{n,ina}^2}{\Delta f} \right) \cdot \frac{R_D^2}{1+\omega^2 R_D^2 C_D^2} \right) + \frac{V_{n,ina}^2}{\Delta f} \right]. \quad (20)$$

When the diode is forward biased, the signal and the noise of the input opamps are transferred by the demodulator circuit due to the low resistance of the diode: $r_{diode} \approx 0$. In this case, the output noise voltage is given by

$$\frac{V_{n,\mathrm{out},fb}^2}{\Delta f} \approx \frac{V_{n,\mathrm{out},ina}^2}{\Delta f} + H_{ina}^2 \cdot \left[\frac{4kTR_G}{\Delta f} + 2\,\frac{V_{n,A}^2}{\Delta f} + \frac{V_{n,ina}^2}{\Delta f} \right]. \quad (21)$$

Every period of $V_{carrier}$ the diode is both reverse biased (about 7/8 part of the period) and forward biased (about 1/8 part of the period), so a combination of (20) and (21) should be used to calculate the total output noise voltage. However, since the diode is reverse biased most of the time and, moreover, when the following condition is met:

$$\frac{V_{n,A}^2}{\Delta f} \le \left(\frac{i_{n,ina}^2}{\Delta f} + \frac{i_{n,diode}^2}{\Delta f} \right) \cdot \frac{R_D^2}{1+\omega^2 R_D^2 C_D^2} \quad (22)$$

then the output noise voltage can be calculated with only (20). Whether or not the condition of (22) is met is dependent on the components and $f_{carrier}$ used.

In a bandwidth $f_2 - f_1$, the total output noise voltage $V_{n,\mathrm{out},tot}$ of the CVC can be calculated with

$$V_{n,\mathrm{out},tot} = \sqrt{\int_{f_1}^{f_2} \frac{V_{n,\mathrm{out}}^2}{\Delta f}\, df}. \quad (23)$$

This noise voltage has to be less than the output voltage of the CVC due to the minimum detectable acceleration of $a = 0.001$ g.

III. Experimental Results and Discussion

A. Components Used and Bridge Balancing Procedure

Two test versions of the CVC were realized with different component values. For the first tests, only fixed capacitors were used instead of the sensor capacitances. When possible, SPICE simulations were carried out.

Version 1: All components are SMD; the opamps are PMI OP237, the inamp is a Burr Brown INA102 ($H_{ina} = 100$), $R_f = 1$ MΩ, $C_{x0} = 12$ pF, C_f is adjustable $5 \cdots 15$ pF ($C_f \approx C_{x0}$), the diodes are BAS 40-06 (Schottky diodes with $V_{diode} = 0.4$ V), $R_D = 18$ kΩ, $C_D = 100$ nF.

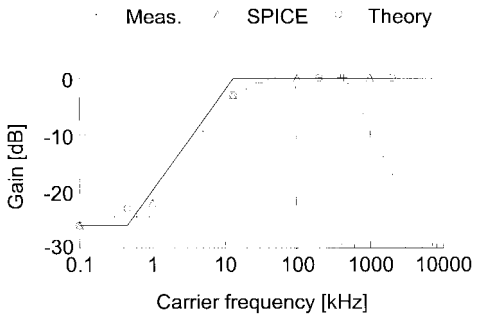

Fig. 5. Bode plot of the transfer function of one of the opamp branches, $V_A/V_{carrier}$; the continuous lines are the asymptotic representation of the theoretically expected values.

Version 2: The opamps are National Semiconductor LF356, the inamp is a Burr Brown INA103 ($H_{ina} = 150$), $R_f = 1$ MΩ, $C_{x0} = 12$ pF, C_f is adjustable $5 \cdots 15$ pF ($C_f \approx C_{x0}$), the diodes are 1N4148 (with $V_{diode} = 0.6$ V), $R_D = 18$ kΩ, $C_D = 100$ nF.

Bridge Balancing Procedure: The supply voltage (±15 V) is switched on and the offset voltage of the inamp is adjusted to zero. The input voltage $V_{carrier}$ is switched on and the two C_f's are adjusted so that V_A and V_B are equal to $-V_{carrier}$ and V_{out} is equal to 0.

B. Dependency of the Transfer Function of the Opamps on the Carrier Frequency

The dependency of the transfer function of the opamps on the carrier frequency $f_{carrier}$ was measured with version 2. In order to imitate a sensor with parasitic components (as shown in Fig. 2), apart from the equivalent sensor capacitance of 12 pF, extra components were added: $C_{p1} = C_{p2} = C'_{p1} = C'_{p2} = 56$ pF, $C_{p3} = C'_{p3} = 5.6$ pF, $R_{pp} = R'_{pp} = 20$ MΩ, and $R_{ps} = R'_{ps} = 2.2\,\Omega$.

The dependency of the transfer function of the opamps on the carrier frequency $f_{carrier}$ was investigated by varying it from 300 Hz up to 2 MHz while the carrier amplitude was kept at 5 V. The resulting transfer function from $V_{carrier}$ to V_A (and V_B) is displayed in Fig. 5.

According to (2)–(4), the expected corner frequencies are 13.0 kHz, 450 Hz, and 5.9 GHz, respectively. The SPICE and measurement results for the lowest two corner frequencies show a good correspondence with the theoretical values. The highest corner frequency is not shown in Fig. 5 and will not be found in practice due to the limited gain bandwidth product and the slew rate (because of the high amplitude) of the opamps used. In the case of version 2, this causes a decrease in the gain at frequencies higher than 400 kHz.

The conclusion can be drawn that when $f_{carrier}$ is in the frequency independent part of the transfer function, small variations in this frequency as well as the parasitic components—both parasitic capacitances and parasitic resistances—do not have any influence on the transfer function. An optimum performance of this part of the circuit is guaranteed when the carrier frequency $f_{carrier}$ is higher than 50 kHz and lower than 400 kHz (in version 2).

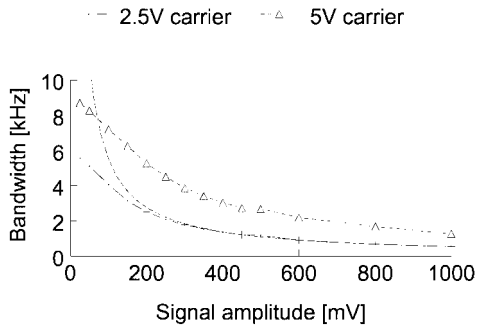

Fig. 6. Measured bandwidth of the CVC versus signal amplitude at two carrier amplitudes; the dashed lines without markers are according to (12) with $K_{2.5\,\mathrm{V}} = 2.4$ and $K_{5\,\mathrm{V}} = 3.0$.

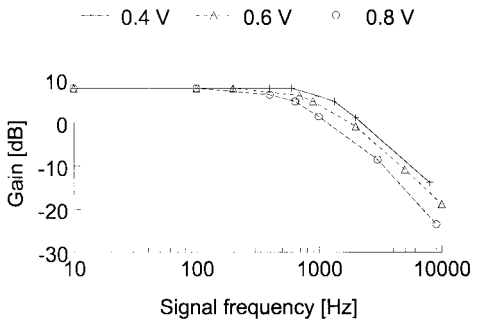

Fig. 7. Measured Bode plot of the CVC at three different signal amplitudes; the dotted horizontal line represents the -3 dB level at $\hat{V}_{carrier} = 2.5$ V.

C. Conversion of Capacitance to Voltage

Since fixed capacitors were used instead of the variable sensor capacitance, an AM voltage V_{AM}, consisting of a carrier sine wave with amplitude $V^{carrier}$ and frequency $f_{carrier}$ and a signal sine wave with amplitude V^{signal} and frequency f_{signal}, instead of $V_{carrier}$ alone, has to be applied to the input in order to test the dynamic response of the circuit. The input voltage of the CVC can now be described with [11]

$$\begin{aligned} V_{\mathrm{AM}} &= (\hat{V}_{carrier} + \hat{V}_{signal} \cos \omega_{signal} t) \cos \omega_{carrier} t \\ &= \hat{V}_{carrier} \left(1 + \frac{\hat{V}_{signal}}{\hat{V}_{carrier}} \cos \omega_{signal} t \right) \cos \omega_{carrier} t. \end{aligned} \tag{24}$$

The output voltage V_{out} of the CVC then becomes, using (17) and changing only one of the two C_{x0}'s in a permanent way by adding a small parallel capacitance ΔC_x

$$V_{\mathrm{out}} = -H_{ina} \hat{V}_{carrier} \frac{\Delta C_x}{C_f} \left(1 + \frac{\hat{V}_{signal}}{\hat{V}_{carrier}} \cos \omega_{signal} t \right) \tag{25}$$

and since only the ac part is to be considered, the dc voltage is filtered out so

$$V_{\mathrm{out}} = -H_{ina} \hat{V}_{signal} \frac{\Delta C_x}{C_f} \cos \omega_{signal} t. \tag{26}$$

The bandwidth of the CVC (version 2) at two values of $V^{carrier}$, 2.5 and 5.0 V, versus V^{signal} is shown in Fig. 6. From Fig. 6 it can be seen that below $V^{signal} = 300$ mV the theoretical bandwidth is higher than the measured bandwidth due to the diode not being forward biased. For $V_{signal} > 300$ mV it can be calculated with (12) that $K_{2.5\,\mathrm{V}} \approx 2.4$ and $K_{5\,\mathrm{V}} \approx 3.0$.

When $\Delta C_x = 0.2$ pF and $V_{carrier} = 2.5$ V, the gain $V_{\mathrm{out}}/V_{signal}$ is expected to be (26) 8.0 dB at low frequencies of V_{signal}. The bandwidth of the circuit is expected to be higher than (8) 88 Hz, the maximum bandwidth should be according to (12). The Bodeplot of the gain of the CVC for three amplitudes of V_{signal}, 400, 600, and 800 mV, is shown in Fig. 7. As can be seen in Fig. 7, at $V^{signal} = 400$ mV $f_{-3\,\mathrm{dB}} = 1350$ Hz, at $V^{signal} = 600$ mV $f_{-3\,\mathrm{dB}} = 920$ Hz and at $V_{signal} = 800$ mV $f_{-3\,\mathrm{dB}} = 620$ Hz which is in good correspondence with (12) with $K_{2.5\,\mathrm{V}} \approx 2.4$.

In the accelerometer case, the signal amplitude caused by a change in capacitance due to an applied acceleration will not exceed 50 mV, so, the specified bandwidth of 50 Hz is guaranteed with this configuration. However, the maximum bandwidth of the circuit will be lower than the value calculated by (12), due to the diode not being forward biased. According to Fig. 6, accelerations with frequencies up to at least 10 kHz can still be detected. By adjusting $V_{carrier}$, R_D, and C_D even higher bandwidths can be obtained.

C. Linearity and Resolution

With a nominal capacitance of 12 pF, it is difficult to realize variations of 2 ppm experimentally (24 aF with respect to 12 pF; however, the SPICE simulations were carried out with these small values). Therefore, the nominal capacitance was increased to 120 nF, the frequency $f_{carrier}$ was decreased to 15 kHz and the amplitude $V^{carrier}$ down to 2 V. In this way a differential capacitance variation of 2 ppm can be realized with two capacitances of 240 fF. This is equal to a single sided capacitance change of 4 ppm or approximately 0.5 pF with respect to 120 nF.

The measurements were carried out with version 2. The capacitance ΔC_x, in parallel with C_{x0}, was varied single sided from 12 nF down to 0.5 pF. The results are shown in Fig. 8(a) and (b); Fig. 8(b) shows the output voltage due to coarse and Fig. 8(a) the output voltage due to fine capacitance variations. The expected theoretical output voltage can be calculated with (17) and is represented in both figures by a line.

Fig. 8(a) and (b) show that the CVC converts capacitance to voltage linearly for both large and small changes in capacitance, respectively. There is a good correspondence between the theory, the SPICE simulations, and the measurements. Note that the accuracy of the absolute value of ΔC_x depends largely on the accuracy and the stability of C_f.

The range in which the relative change in capacitance is linearly detected can be increased by decreasing $V^{carrier}$ and H_{ina}. However, the signal to noise ratio is decreased when $V^{carrier}$ is decreased.

D. Stability

Version 1 was used to measure the drift during a certain period of time, with $\Delta C_x = \Delta C_x' = 0$. The circuit was placed

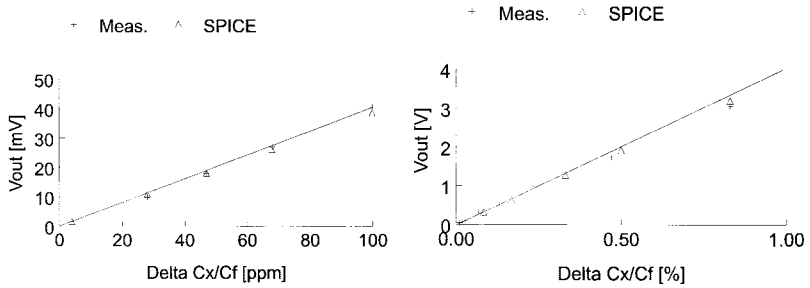

(a) (b)

Fig. 8. Measured and simulated output voltage versus relative change in capacitance (a) fine and (b) coarse. The continuous line is according to (17).

in a shielded box at ambient temperature. An input voltage with $f_{carrier} = 100$ kHz and $V^{carrier} = 10$ V was applied and the output signal $V_{\rm out}$ was set to 0 V. After 18 h, it was still 0 V, with small slow fluctuations with a maximum amplitude of 7 mV. The maximum amplitude of the fluctuations equals, respectively, 7 ppm single sided and 3.5 ppm differential. This means that in time an absolute accuracy and resolution of 3.5 ppm is possible. The fluctuations in the output voltage are caused by inequalities in the diode behavior.

E. Noise

The spectral density of the output noise of the circuit was measured with a spectrum analyzer (HP 35 670A dynamic signal analyzer), the rms output noise voltage with a measuring amplifier (Brüel & Kjaer 2610). The noise measurement was done with version 1 with $\Delta C_x = \Delta C_x = 0$.

According to the specifications of the INA102 at $H_{ina} = 100$, this instrumentation amplifier has an equivalent input noise voltage $V_{n,\,ina}$ which decreases from 60 nV/$\sqrt{\rm Hz}$ at 1 Hz to 25 nV/$\sqrt{\rm Hz}$ at 100 Hz. Its equivalent input noise current $i_{n,\,ina}$ decreases from 1.2 pA/$\sqrt{\rm Hz}$ at 1 Hz to 0.2 pA/$\sqrt{\rm Hz}$ at 100 Hz.

At 100 kHz, the OP237 has a specified noise voltage $V_{n,\,op}$ of 3.2 nV/$\sqrt{\rm Hz}$ and a noise current $i_{n,\,op}$ of 0.4 pA/$\sqrt{\rm Hz}$. Using (18), with this opamp at this carrier frequency the condition as set in (22) is not fulfilled, so the total output noise voltage can not be approximated with (20). However, when $f_{carrier}$ is increased and R_f is decreased, it is possible to meet the condition as set in (22).

Using the specifications, the noise levels can be calculated. The results of both calculation and measurement are shown in Fig. 9.

From Fig. 9 it can be seen that the measured output noise voltage density $V_{n,\,\rm out}$ when $V^{carrier} = 0$ (the diodes are reverse biased) is in good correspondence with the theory. The total rms output noise voltage was measured in the frequency range 2–50 Hz and was found to be 150 μV which is also in good correspondence with the calculated (20), (23) and measured values. In normal operation, when $V^{carrier} = 10$ V, the measured rms noise voltage was 750 μV instead of the calculated 210 μV (20), (21), (23). The mismatch is due to the low frequency noise of the opamps which was assumed to be suppressed by the dominant high carrier frequency $f_{carrier}$, but is nevertheless present. However, when a high pass filter is added in between the opamp and the diode, the low frequency noise of the opamps should be rejected so that the rms noise voltage will be reduced to the calculated value of 210 μV. It should be noted that this measure is not necessary as long as the resulting rms output noise voltage is less than the output signal voltage due to the lowest acceleration to be detected.

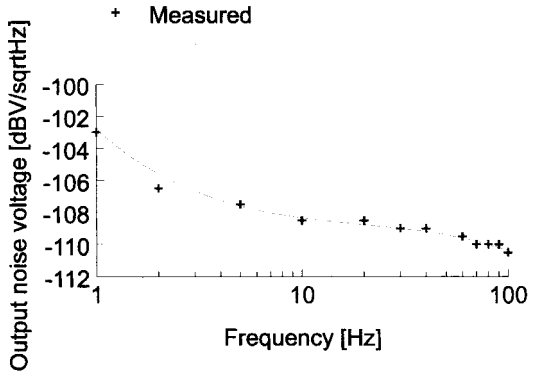

Fig. 9. Measured (markers) and calculated [dotted line, according to (20)] output noise voltage density of the CVC with $\hat{V}_{carrier} = 0$.

F. CVC with Sensor

The sensor of Fig. 1 [8], [9] is connected to the CVC of version 1. The input voltage $V_{carrier}$ has a frequency $f_{carrier} = 100$ kHz and an amplitude $V^{carrier} = 10$ V. The resulting sensitivity of the accelerometer is 4.0 V/g. The signal to noise ratio at 1 g in the signal bandwidth 2 Hz to 50 Hz is therefore $20.\log(4.0/750\,\mu) = 75$ dB. The signal to noise ratio at the lowest acceleration to be detected 0.001 g in the same bandwidth is $20.\log(0.004/750\,\mu) = 15$ dB, so, it is not necessary to put high pass filters in between the opamps and the diodes. However, the signal to noise ratio will be improved to $20.\log(4.0/210\,\mu) = 86$ dB instead of 75 dB when the high pass filters would be used.

IV. Conclusions

In this paper, a sensitive differential capacitance to voltage converter (CVC) has been presented which can for instance be used with a differential capacitive accelerometer. The CVC is completely symmetrical and consists of two frequency independent half ac-bridges which act as AM modulators,

two AM demodulators consisting of a diode and an RC-filter and an instrumentation amplifier which rejects common mode signals. The specific advantages of this CVC compared to other CVC's are that it is intrinsically immune to parallel and serial parasitic resistances and capacitances, that it can measure both statical and dynamical variations in capacitances in the wide frequency range from dc up to at least 10 kHz, that undesired common mode signals are rejected because of the high degree of symmetry in the circuit and that it can be easily realized with discrete components. The signal bandwidth can be enlarged by increasing $V^{carrier}$ and decreasing the demodulation resistor R_D and the demodulation capacitor C_D.

A detectable change in capacitance is 2 ppm (in the accelerometer case 24 aF with respect to 12 pF). The absolute accuracy and stability was measured to be 3.5 ppm. The CVC is linear within relative capacitance changes of 2 ppm and 1%, thus having a dynamic range of at least 74 dB. The rms output noise voltage is dominated by the low frequency noise of the opamps and was measured to be 750 μV in the frequency range of 2 Hz to 50 Hz. The noise voltage can be reduced to 210 μV by putting high pass filters in between the opamps and the diodes.

The differential capacitive accelerometer is well-functioning with this CVC, with a signal to noise ratio of 75 dB at an acceleration of 1 g in the frequency range 2 Hz to 50 Hz. Furthermore, all measurement results showed a good correspondence with the theoretical analyses.

ACKNOWLEDGMENT

The authors would like to thank technician E. A. Droog for his assistance in the preparation of the electronic circuitry, Dr. P. P. L. Regtien for his careful reading of the manuscript, and students Ö. Mesut, B. Bakanyildiz, O. Öztürk, and Z. Sönmez for their theoretical and experimental work.

REFERENCES

[1] S. M. Huang, A. L. Stott, R. G. Green, and M. S. Beck, "Electronic transducers for industrial measurement of low value capacitance," *J. Phys. E: Sci. Instrum.*, vol. 21, pp. 242–280, 1988.
[2] R. Pallás-Areny and J. G. Webster, *Sensors and Signal Conditioning.* New York: Wiley, 1992.
[3] D. Marioli, E. Sardini, and A. Taroni, "Measurement of small capacitance variations," *IEEE Trans. Instrum. Meas.*, vol. 40, Apr. 1991.
[4] F. N. Toth and G. C. M. Meijer, "A low-cost, smart capacitive position sensor," *IEEE Trans. Instrum. Meas.*, vol. 41, Dec. 1992.
[5] M. Yamada, T. Takebayashi, S. I. Notoyama, and K. Watanabe, "A switched-capacitor interface for capacitive pressure sensors," *IEEE Trans. Instrum. Meas.*, vol. 41, Feb. 1992.
[6] W. C. Heerens, "Application of capacitance techniques in sensor design," *Phys. E: Sci. Instrum.*, vol. 19, 1986.
[7] J. C. Lötters, W. Olthuis, P. H. Veltink, and P. Bergveld, "On the design of a triaxial accelerometer," *J. Micromech. Microeng.*, vol. 5, pp. 128–131, 1995.
[8] ——, "Polydimethylsiloxane as an elastic material applied in a capacitive accelerometer," *J. Micromech. Microeng.*, vol. 6, pp. 52–54, 1996.
[9] ——, "Design and feasibility of a symmetrical triaxial capacitive accelerometer for medical purposes," in *Proc. Eurosensors X*, Leuven, Belgium, Sept. 1996, pp. 441–444.
[10] P. R. Gray and R. G. Meyer, *Analysis and Design of Analog Integrated Circuits*, 2nd. ed. New York: Wiley, 1984.
[11] E. Stadler, "Modulationsverfahren," Vogel-Buchverlag, Wuerzburg, 4, Auflage, 1986.

Joost C. Lötters was born in Doetinchem, The Netherlands, on July 20, 1967. He received the B.Sc. degree in electrical engineering from the Technical Institute Arnhem, Arnhem, The Netherlands, in 1990, the M.Sc. degree in 1993, and the Ph.D. degree in 1997 in electrical engineering from the University of Twente, Enschede, The Netherlands. The title of his Ph.D. dissertation is "A highly symmetrical capacitive triaxial accelerometer," which deals with the design, fabrication, characterization, and application of a miniature and eventually implantable triaxial accelerometer for biomedical purpose. Possible applications of the device are the control of mobility in paraplegic patients and the monitoring of movement disorders of patients suffering from Parkinson's disease.

In 1997, he joined the Research Department, Bronkhorst High-Tech, Ruurlo, The Netherlands.

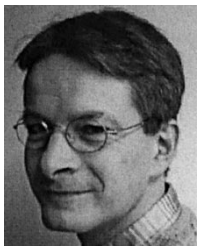

Wouter Olthuis was born in Apeldoorn, the Netherlands, on October 23, 1960. He received the M.S. degree in electrical engineering from the University of Twente, Enschede, The Netherlands, in 1986, and the Ph.D. degree from the Biomedical Engineering Division, Faculty of Electrical Engineering, University of Twente, in 1990. The subject of his dissertation was the use of iridium oxide in ISFET-based coulometric sensor-actuator devices.

Currently, he is an Assistant Professor, Laboratory of Biosensors, MESA Research Institute, University of Twente.

Peter H. Veltink (S'85–M'88) received the M.Sc. degree in electrical engineering from the University of Twente, Enschede, The Netherlands, in 1984 and the Ph.D. degree in 1988. His dissertation topic was recruitment of myelinated nerve fibers during artificial nerve stimulation.

He is a faculty member, Signals and Systems Department, Faculty of Electrical Engineering, University of Twente, and is affiliated with the Institute for Biomedical Technology at the same university. His research is in the area of artificial motor control, specifically related to functional neuromuscular stimulation and the application of body mounted sensors for human movement analysis. In 1989, he was a Visiting Assistant Professor, Case Western Reserve University, Cleveland, OH, and in 1997 and 1998, he was on sabbatical at the Center for Sensory-Motor Interaction, Aalborg University, Denmark. He is the Scientific Coordinator of the NEUROS Project, Training and Mobility of Researchers Program, European Union, and Treasurer of the International Functional Electrical Stimulation Society.

Dr. Veltink received the Royal Shell Stimulating Prize for his contribution to the rehabilitation engineering field in 1997.

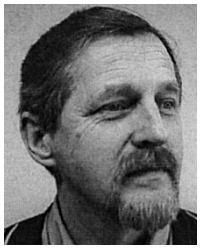

Piet Bergveld was born in Oosterwolde, The Netherlands, on January 26, 1940. He received the M.Sc. degree in electrical engineering from the University of Eindhoven, Eindhoven, The Netherlands, in 1965 and the Ph.D. degree from the University of Twente, Enschede, The Netherlands, in 1973. The subject of his dissertation was the development of ISFET's and related devices. Since then, the actual invention of the ISFET has been investigated by many international research groups as well as industry.

Since 1965, he has been a member of the Biomedical Engineering Division, Faculty of Electrical Engineering, University of Twente, and, in 1984, he was appointed Full Professor in biosensor technology. He is one of the project leaders in the MESA Research Institute. His research subjects still concern the further development of ISFET's and biosensors based on ISFET technology as well as physical sensors for biomedical and environmental applications, resulting in more than 300 papers.

Dr. Bergveld was recently appointed as a member of the Royal Dutch Academy of Science.